Petroleum Science 23 (2026) 5081–5095

Contents lists available at ScienceDirect

Petroleum Science

journal homepage: www.keaipublishing.com/en/journals/petroleum-science

Original Paper

A new model to predict the electrical submersible Pump's characteristic curves under highly viscous flow

William Monte Verde [a,*], Ellen Kindermann [b], Natan Augusto Vieira Bulgarelli [a], Bernardo Foresti [c], Antonio Carlos Bannwart [a]

[a] Center for Energy and Petroleum Studies, University of Campinas, São Paulo, Brazil
[b] School of Mechanical Engineering, University of Campinas, São Paulo, Brazil
[c] Cenpes, Petrobras, Rio de Janeiro, Brazil

ARTICLE INFO

Article history:
Received 5 February 2025
Received in revised form
22 October 2025
Accepted 25 February 2026
Available online 3 March 2026

Edited by Xi Zhang

Keywords:
Electrical submersible pump (ESP)
Viscous flow
Performance degradation
Performance prediction
Correction factors
Empirical model

ABSTRACT

Electrical submersible pumps (ESP) are a key artificial lift method, particularly in challenging oilfield operations involving highly viscous fluids such as heavy oil, emulsions, or subsea boosting applications. Traditional empirical models for predicting ESP performance often face significant limitations, including substantial deviations due to reliance on restricted datasets. This study presents a novel prediction model addressing these challenges by leveraging a comprehensive experimental dataset encompassing diverse operating conditions, fluid viscosities, and impeller geometries. The model predicts single-stage performance curves and extends applicability to multi-stage ESPs through isothermal and non-isothermal approaches, incorporating energy dissipation effects. Validation against experimental data demonstrates accurate predictions for head, flow rate, and efficiency, significantly reducing errors compared to existing methods. Additionally, the prediction model and multi-stage approaches were tested with datasets from other authors. Even when applied to different ESP geometries, the model demonstrated good accuracy in estimating correction factors and predicting complete performance curves.

1. Introduction

In challenging oilfield operations, artificial lift methods are essential for improving oil production or ensuring its economic feasibility. These operations often involve complex fluids and flow dynamics, such as multiphase mixtures and emulsions. One of the most widely used artificial lift methods is the electrical submersible pump (ESP) system. Typically, the term "ESP system" refers to the complete assembly, including the pump, electric motor, seal, and instrumentation, while "ESP" specifically refers to the multi-stage pump. Xiao et al. (2020) estimated that approximately 130000 ESP systems are installed worldwide, contributing to around 60% of the total global oil production. This widespread use highlights the critical role of ESP systems in sustaining and enhancing oil flow rates, particularly in heavy oilfields and mature oilfields with increasing water production.

One of the main advantages of the ESP system is its flexibility, which allows for various completions and configurations. In traditional applications, the ESP system is installed downhole. Although these systems operate effectively, intervention costs remain a significant concern. To address this issue, different subsea boosting systems have been developed, including vertical booster stations, horizontal booster stations, and jumper systems (Colodette et al., 2008; Costa et al., 2013; Homstvedt et al., 2015). Some of these subsea boosting systems use the same multi-stage centrifugal pumps and other components as those used in traditional downhole ESP systems, commonly referred to as ESP booster systems. However, flow assurance is a critical challenge for any seafloor installation (Kumar, 2023). In such applications, the lower pressure and temperature at the ESP intake can result in challenges such as high viscosities, hydrate formation, and slugging.

The hydraulic challenges faced by ESPs are directly related to the fluid properties. In general, in any fluid or flow characteristic that deviates from low-viscosity and single-phase liquid operation

* Corresponding author.
E-mail address: wmv@unicamp.br (W. Monte Verde).
Peer review under the responsibility of China University of Petroleum (Beijing).

https://doi.org/10.1016/j.petsci.2026.02.020

inevitably impacts the performance of this equipment (Monte Verde et al., 2017; Bulgarelli et al., 2022b). The temperature-related issues encountered in ESP booster systems, heavy oil production, or the presence of emulsions result in highly viscous flow, which is one of the primary factors impairing the performance of centrifugal pumps. Higher viscosity intensifies friction losses and viscous shear within the impeller and diffuser channels, reducing the head and increasing the shaft power due to the rise in disk losses (Bulgarelli et al., 2022a; Gülich, 2008). Oversizing the hydraulic capacity of the ESP becomes necessary to handle a specified flow rate and compensate for the reduced performance. When the fluid viscosity increases significantly due to seabed temperatures after a system shutdown, the probability of a difficult restart or even pump shaft failure rises (Monte Verde et al., 2021). Therefore, determining the performance of ESPs operating under viscous flow is essential not only for pump system design but also for operation, which helps prevent failures and improves efficiency.

Even so, manufacturers typically provide characteristic curves for head, brake horsepower (BHP), and efficiency based on standard operation with water. Deviations caused by viscosity are usually addressed using corrections or computational fluid dynamics (Stel et al., 2015; Wang et al., 2024; Yang et al., 2024), since testing these systems with real fluids is costly, time-consuming, and therefore uncommon. In parallel, recent studies have also investigated the use of machine learning and optimization techniques for pump performance prediction, including adaptive support vector regression and bio-inspired algorithms such as the whale optimization algorithm (Lin et al., 2024; Zhou et al., 2025; Luo et al., 2025). These approaches show promising results, particularly for centrifugal and vortex pumps, but their application has so far been mostly limited to low-to-moderate viscosity conditions. Consequently, the prediction of ESP performance under viscous flow still presents several technical gaps, especially in the development of specific and generalized models applicable to various impeller geometries and viscosity ranges.

The present work continues the studies presented by Monte Verde et al. (2023, 2024), which aim to address these gaps and provide new contributions to this topic. In the first study, Monte Verde et al. (2023) conducted an experimental investigation to characterize the performance of ESPs operating with viscous fluids. A total of six models of three-stage ESPs, from two diameter series, were tested. The tests also covered four speeds, ranging from 1800 to 3500 rpm, eleven viscosities, varying from 24 to 1273 cP, resulting in a comprehensive database of over 5800 operating conditions. Table 1 summarizes the key characteristics of the experimental dataset used for model development, as originally detailed in Monte Verde et al. (2023).

This database contributed to the literature given the lack of available open data. Additionally, the authors conducted a phenomenological analysis of the influence of operational parameters, such as viscosity, rotational speed, specific speed, and rotational Reynolds number. As a result of these phenomenological analyses, valuable insights were obtained and utilized in this study to develop the proposed simplified prediction model.

Table 1
Characteristics of the experimental dataset (Monte Verde et al., 2023).

Parameter	Range
Pump models	P37, P47, P62, P100, HC10000, HC12500
Series	538, 675
Impeller diameter, mm	108, 134
Stage number	3
Dynamic viscosity, cP	1, 24, 50, 88, 128, 226, 330, 474, 655, 847, 1036, 1273
Rotational speed, rpm	1800, 2400, 3000, 3500

In sequence, Monte Verde et al. (2024) conducted a critical assessment of the available models proposed by Stepanoff (1949); KSB (1989); Gülich (2008); ANSI-HI (2010); Monte Verde (2016) and Ofuchi et al. (2020), which are used for predicting the performance of ESPs under viscous conditions. The significant errors observed in the predictions highlighted the limitations of these models, primarily attributed to their reliance on databases predominantly derived from conventional centrifugal pumps. Subsequently, the authors modified these original models based on the database provided by Monte Verde et al. (2023). The accuracy of the modified models significantly improved following these adjustments. Despite the substantial improvement in the accuracy of the modified models, the authors highlight a key limitation: most of these models address only the performance at the best efficiency point (BEP) and are unable to provide complete degraded performance curves, which are essential for system design. Furthermore, the authors recommend that the models incorporate the specific speed and investigate alternative functional relationships to improve prediction accuracy.

This work proposes a new performance prediction model specifically developed for ESPs that can estimate performance curves for head, BHP, and efficiency. To achieve this, insights from previous studies and the experimental open database of Monte Verde et al. (2023) were utilized to calibrate the mathematical model. This work also proposes approaches to apply the model to multi-stage pumps, accounting for energy dissipation during pumping. The proposed model and these approaches were validated using performance data from other authors. The main contribution of this study is the proposal of an analytical model that uses easily obtainable input data, enabling straightforward application and integration into flow simulation software via user-defined functions.

The main novelty of this work is the development of a generalized prediction model specifically derived from ESP viscous performance data, capable of reconstructing the entire characteristic curves (head, efficiency, and flow rate). Unlike existing empirical correlations, which were mostly developed for conventional centrifugal pumps, the proposed model accounts for pump specific speed and extends its validity to highly viscous conditions. In contrast with CFD-based methods, it requires only standard operating parameters, ensuring computational efficiency and straightforward integration into production simulators.

2. Performance prediction procedure

This section presents a new empirical model proposed to estimate the performance of ESPs under viscous flow. The model was developed to predicts single-stage performance curves, considering only one impeller and diffuser set. Since ESPs generally consist of multiple stages, two approaches are also proposed to extend the model for such conditions. This section introduces these approaches, which consider isothermal and non-isothermal flow.

2.1. Model fundamentals

The viscous curve is obtained based on six characteristic points. The first step of the procedure is to calculate these points and the second involves adjusting the complete pump curve. The correspondence between the points on the reference curves with water (in blue) and those on the degraded curve (in black) are shown in Fig. 1. This figure shows the curves of efficiency (η) and head (H) as a function of flow rate (Q), with the subscripts w and vis

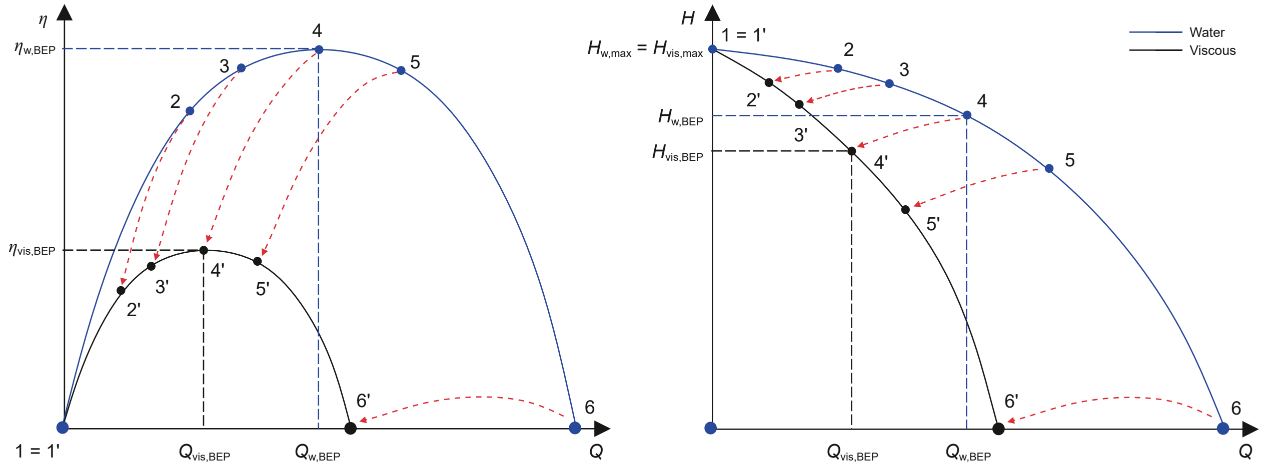

Fig. 1. Correspondence between the points on the reference curve with water and the points on the curve during viscous operation.

representing operation with water and viscous fluid, respectively. Each characteristic point on the water curve (1 to 6) has a corresponding point on the operating curve with a viscous fluid (1′ to 6′). In the operating curve with water, Point 1 refers to the shut-off, where the flow rate and efficiency are zero, and the head is at its maximum. Point 4 corresponds to the BEP. Points 2, 3, and 5 represent conditions where the flow rates are equivalent to 60%, 80%, and 120% of the BEP flow rate, respectively. Finally, Point 6 represents the open-flow, a condition of maximum flow rate and zero head and efficiency. These points are summarized in Table 2. The subscripts 0.6, 0.8, and 1.2 of BEP represent the operating flow rate relative to the BEP. All these values are assumed as input data for the prediction model and can be obtained from the operating curves provided by the manufacturer or from independent tests with water.

The corresponding operational points of the viscous curve follow an analogous approach to those of the curve with water. Table 3 summarizes the characteristic points of the viscous curve. Regarding Point 1′, an important assumption is made: the head at the shut-off condition is the same for both water and viscous fluid operations. This simplification is consistent with turbomachinery theory, as Euler's equation indicates that the theoretical head is governed by impeller geometry and peripheral velocity, and at zero flow rate the viscous effects do not significantly alter the energy transfer. Moreover, this consideration is supported by the experimental data presented by Monte Verde et al. (2023), which show a negligible variation in the shut-off head as a function of viscosity. A similar treatment can be found in Gülich (2008) and Stepanoff (1949) in their modeling of centrifugal pump performance.

The prediction of viscous operation is carried out using correction factors, which are defined as the ratio between viscous performance and water performance at corresponding points. The flow rate correction factor at the BEP ($C_{Q,\mathrm{BEP}}$) is determined by the ratio of the viscous flow rate at BEP to the water flow rate at BEP:

Table 2
Characteristic points on the water performance curve.

	Point 1	Point 2	Point 3	Point 4	Point 5	Point 6
Q_w	0	$0.6\ Q_{w,\ BEP}$	$0.8\ Q_{w,BEP}$	$Q_{w,BEP}$	$1.2\ Q_{w,BEP}$	$Q_{w,max}$
H_w	$H_{w,max}$	$H_{w,0.6BEP}$	$H_{w,0.8BEP}$	$H_{w,BEP}$	$H_{w,1.2BEP}$	0
η_w	0	$\eta_{w,0.6BEP}$	$\eta_{w,0.8BEP}$	$\eta_{w,BEP}$	$\eta_{w,1.2BEP}$	0

$$C_{Q,\mathrm{BEP}} = \frac{Q_{\mathrm{vis,BEP}}}{Q_{\mathrm{w,BEP}}} \tag{1}$$

For any flow rate related to the BEP, e.g. point 2′, which corresponds to 60% of the BEP flow rate, the correction factor is given by $0.6\ Q_{\mathrm{vis,BEP}}/0.6\ Q_{\mathrm{w,BEP}}$, which results in the correction factor for the BEP. Therefore, flow rate correction factors for other conditions related to the BEP, such as points 3′, 4′, and 5′, can be generalized as:

$$C_{Q,0.6\mathrm{BEP}} = C_{Q,0.8\mathrm{BEP}} = C_{Q,1.2\mathrm{BEP}} = C_{Q,\mathrm{BEP}} \tag{2}$$

Thus, at a constant rotational speed, the flow rate correction coefficients calculated at the BEP and at any operational flow rate that is related to the BEP have the same value by definition, obtaining:

$$C_{Q,\mathrm{BEP}} = \frac{Q_{\mathrm{vis,0.6BEP}}}{Q_{\mathrm{w,0.6BEP}}} = \frac{Q_{\mathrm{vis,0.8BEP}}}{Q_{\mathrm{w,0.8BEP}}} = \frac{Q_{\mathrm{vis,BEP}}}{Q_{\mathrm{w,BEP}}} = \frac{Q_{\mathrm{vis,1.2BEP}}}{Q_{\mathrm{w,1.2BEP}}} \tag{3}$$

A different behavior is observed at the maximum flow rate condition, which exhibits a flow rate correction factor greater than the others, as discussed by Monte Verde et al. (2023). Therefore, a specific flow rate correction factor ($C_{Q,\max}$) is defined as the open flow condition.

$$C_{Q,\max} = \frac{Q_{\mathrm{vis,max}}}{Q_{\mathrm{w,max}}} \tag{4}$$

Neglecting changes in kinetic and potential energy across the pump stage, the net head is essentially equal to the change in pressure head:

$$H = \frac{\Delta P}{\rho g} \tag{5}$$

where ΔP is the stage pressure increment, ρ is the fluid density, and g is the gravitational acceleration. The impaired stage head for the shut-off (1′) and open-flow (6′) points are defined in Table 3. For the other conditions, the head correction factors (C_H) are defined as:

$$C_{H,0.6\mathrm{BEP}} = \frac{H_{\mathrm{vis,0.6BEP}}}{H_{\mathrm{w,0.6BEP}}} \tag{6}$$

Table 3
Characteristic points on the viscous performance curve.

	Point 1′	Point 2′	Point 3′	Point 4′	Point 5′	Point 6′
Q_{vis}	0	0.6 $Q_{vis,BEP}$	0.8 $Q_{vis,BEP}$	$Q_{vis,BEP}$	1.2 $Q_{vis,BEP}$	$Q_{vis,max}$
H_{vis}	$H_{vis,max} = H_{w,max}$	$H_{vis,0.6BEP}$	$H_{vis,0.8BEP}$	$H_{vis,BEP}$	$H_{vis,1.2BEP}$	0
η_{vis}	0	$\eta_{vis,0.6BEP}$	$\eta_{vis,0.8BEP}$	$\eta_{vis,BEP}$	$\eta_{vis,1.2BEP}$	0

$$C_{H,0.8BEP} = \frac{H_{vis,0.8BEP}}{H_{w,0.8BEP}} \tag{7}$$

$$C_{H,BEP} = \frac{H_{vis,BEP}}{H_{w,BEP}} \tag{8}$$

$$C_{H,1.2BEP} = \frac{H_{vis,1.2BEP}}{H_{w,1.2BEP}} \tag{9}$$

The pump stage efficiency is defined as the ratio of the useful power delivered to the fluid (P_h) to the power required to drive the pump stage, the BHP:

$$\eta = \frac{P_h}{BHP} = \frac{\rho g H Q}{\omega \Gamma} \tag{10}$$

where ω is the rotational speed and Γ is the shaft torque. The efficiency under viscous flow is zero at the shut-off (1′) and open-flow (6′) points, since the flow rate and head are zero, respectively. For the other characteristic points, Monte Verde et al. (2023) showed that the efficiency correction factors (C_η) are practically constant for points 2′, 3′, 4′, and 5′:

$$C_\eta = C_{\eta,0.6BEP} = C_{\eta,0.8BEP} = C_{\eta,BEP} = C_{\eta,1.2BEP} \tag{11}$$

Therefore, it is assumed that a single efficiency correction factor is valid for predicting the efficiency at the BEP and flow rates equivalent to 60%, 80%, and 120% of the BEP flow rate, yielding:

$$C_\eta = \frac{\eta_{vis,0.6BEP}}{\eta_{w,0.6BEP}} = \frac{\eta_{vis,0.8BEP}}{\eta_{w,0.8BEP}} = \frac{\eta_{vis,BEP}}{\eta_{w,BEP}} = \frac{\eta_{vis,1.2BEP}}{\eta_{w,1.2BEP}} \tag{12}$$

2.2. Proposed model for ESPs performance under viscous flow

The correction factors are calculated based on empirical correlations. In this study, these correlations are proposed driven by the experimental database and conclusions presented by Monte Verde et al. (2023), as well as the assessments of available prediction models conducted by Monte Verde et al. (2024).

An important finding presented by Monte Verde et al. (2023) is that, for constant rotation and viscosity, the viscous correction factors increase with the specific speed of the ESPs. This indicates that more radial ESPs experience greater performance degradation due to viscosity, while axial ESPs are less affected. This highlights the need for prediction models to account for the specific speed of the ESPs, a factor not considered in the models currently available in the literature.

In turn, Monte Verde et al. (2024) demonstrated that the common direct correlation between C_Q and C_H, used by different authors such as Stepanoff (1949), Gülich (2008), ANSI-HI (2010), and Ofuchi et al. (2020), is inadequate for capturing the experimental database. This also invalidates Stepanoff's hypothesis, which suggests that pump performance degradation at the BEP occurs while maintaining a constant specific speed, leading to $C_{Q,BEP} = C_{H,BEP}^{1.5}$. Therefore, the key insight proposed by the authors is that the correlations for calculating C_Q and C_H must be independent.

The development of the proposed model was based on these previous findings. Different functional relationships for the model were tested. During these tests, the empirical constants were adjusted to minimize the error between the predicted and measured correction factors, provided by the ESP performance database from Monte Verde et al. (2023). The optimization of the coefficients was performed using the Levenberg–Marquardt (LM) method. The LM algorithm is an iterative procedure designed to minimize a sum of squared errors, combining the advantages of two classical optimization techniques: gauss–newton and gradient descent. The optimization codes were implemented in Python using the SciPy library. The model was optimized by minimizing the root mean squared error (RMSE), defined as follows:

$$RMSE = \sqrt{\frac{1}{n}\sum_{i=1}^{n}(\widehat{y}_i - y_i)^2} \tag{13}$$

where $y_i = y_1, y_2, \ldots, y_n$ is a dataset of experimental correction factors, $\widehat{y}_i = \widehat{y_1}, \widehat{y_2}, \ldots, \widehat{y_n}$ is a dataset of predicted correction factors, for n measured data. The RMSE quantifies the average magnitude of prediction errors and is particularly sensitive to large deviations. It is calculated as the square root of the mean of the squared differences between predicted and observed values, with lower RMSE values indicating better predictive accuracy.

In addition to RMSE, other statistical parameters are considered to quantify the accuracy of the proposed model's predictions, such as the absolute relative error (e_r), mean absolute percentage error (MAPE), and coefficient of determination (R^2). The e_r measures the absolute difference between the predicted and observed values relative to the observed value, providing a normalized indication of error for each individual prediction. This metric is particularly useful for identifying localized discrepancies, especially in datasets with wide-ranging magnitudes. Lower values indicate that the predicted values are closer to the actual data. The MAPE expresses the average absolute difference between predicted and observed values as a percentage of the observed values. It is particularly useful for interpreting the model's performance in relative terms and is scale-independent. A lower MAPE indicates that the model's predictions are, on average, closer to the actual values. The R^2 measures the proportion of the variance in the observed data that is explained by the model, where values closer to 1 indicate a better fit. These variables are defined as follows:

$$e_r = \frac{|\widehat{y}_i - y_i|}{y_i} \times 100 \tag{14}$$

$$MAPE = \frac{1}{n}\sum_{i=1}^{n}\frac{|\widehat{y}_i - y_i|}{y_i} \times 100 \tag{15}$$

$$R^2 = 1 - \frac{\sum_{i=1}^{n}(y_i - \widehat{y}_i)^2}{\sum_{i=1}^{n}(y_i - \overline{y}_i)^2} \tag{16}$$

where $\overline{y_i}$ is the mean of a sample with n measured data. Each statistical parameter provides different information and must be analyzed together.

Although dividing datasets into training and test sets is a common practice to reduce bias and improve the reliability of predictive models, the dataset used in this study is relatively small for such a division. Nonetheless, tests were performed, with 70.2% of the experimental data allocated for training and the remaining 29.8% used for testing. The differences observed between this approach and using the entire dataset for optimization were minimal. Therefore, optimizations were performed using the entire database.

The proposed correlations are a function of the dimensionless parameter B, defined as:

$$B = \left(\frac{1}{\omega_s} \frac{\omega\, Q_{\mathrm{w,BEP}}}{\nu \sqrt{g H_{\mathrm{w,BEP}}}} \right)^{0.298} \tag{17}$$

where ω is the rotational speed in rad/s, $Q_{\mathrm{w,BEP}}$ is the water flow rate at BEP in m^3/s, ν is the kinematic viscosity of the viscous fluid in m^2/s, $H_{\mathrm{w,BEP}}$ is the stage head with water at the BEP in m, and ω_s is the dimensionless specific speed of the pump:

$$\omega_s = \frac{\omega\, Q_{\mathrm{w,BEP}}^{1/2}}{\left(g H_{\mathrm{w,BEP}}\right)^{3/4}} \tag{18}$$

The dimensionless parameter B adopted in this work is a modification of the parameter originally introduced by the ANSI/HI 9.6.7-2010 standard for viscous corrections in centrifugal pumps. In the present formulation, the specific speed ω_s was incorporated into the definition of B, so that the influence of pump geometry is directly included in the correlations. Physically, B may be interpreted as a similarity parameter that balances inertial and viscous effects at the pump scale. Higher viscosity increases viscous dissipation and therefore lowers B, whereas higher rotational speed or flow rate increase inertial dominance and raise B. The explicit dependence on specific speed reflects the trend that radial pumps (low ω_s) are more sensitive to viscous degradation than mixed-flow or axial pumps (higher ω_s). In this sense, the modified B functions as a geometry-aware Reynolds-type number that condenses viscosity, rotational speed, and impeller geometry into a single parameter.

The flow rate correction factor, valid for the 0.6, 0.8, 1.0, and 1.2 of BEP, is given by:

$$C_Q = B^{-\left(\frac{35.383}{B^{2.438}}\right)} \tag{19}$$

and the correction factor related to maximum flow rate, defined in Eq. (4), is:

$$C_{Q,\max} = B^{-\left(\frac{24.050}{B^{2.274}}\right)} \omega_s^{-0.161} \tag{20}$$

The head correction factor is a function of parameter B and the ratio of the operational flow rate to the BEP flow rate:

$$C_H = 1 - \left[1 - B^{-\left(\frac{20.033}{B^{2.525}}\right)}\right] \left(\frac{Q_{\mathrm{w}}}{Q_{\mathrm{w,BEP}}}\right)^{0.421} \tag{21}$$

where $Q_{\mathrm{w}}/Q_{\mathrm{w,BEP}}$ is 0.6, 0.8, 1, and 1.2 for $C_{\mathrm{H,0.6BEP}}$, $C_{\mathrm{H,0.8BEP}}$, $C_{\mathrm{H,BEP}}$ and $C_{\mathrm{H,1.2BEP}}$, respectively.

The efficiency correction factor is calculated as:

$$C_\eta = B^{-\left(\frac{59.293}{B^{2.295}}\right)} \tag{22}$$

The database used to adjust the proposed model consists of the following ranges: $0.65 < \omega_s < 1.17$, $11.5 < Q_{\mathrm{w,BEP}} < 83.8$ m^3/h, $3.3 < H_{\mathrm{w,BEP}} < 29.5$ m, $20 < \nu < 1020$ mm^2/s, and $1800 < \omega < 3500$ rpm, resulting in $4.76 < B < 19.02$ for the dimensionless parameter B. It is important to note that the proposed prediction model is valid for a single ESP stage. Therefore, when calculating parameter B and the other parameters, unitary performance from a single stage is considered.

Once the performance with water is known and the correction factors are obtained from the proposed empirical correlations, the operational characteristics with viscous fluid, i.e. H_{vis}, Q_{vis} and η_{vis}, can be calculated to obtain the necessary values in Table 3, thereby completing the prediction of points 1′ to 6′.

Since the characteristic points under viscous flow 1′ to 6′ are defined, the performance curves $H_{\mathrm{vis}} \times Q_{\mathrm{vis}}$ and $\eta_{\mathrm{vis}} \times Q_{\mathrm{vis}}$ can be adjusted. As a standard procedure, a second-order polynomial fit is recommended for the head versus flow curve, while a third-order polynomial fit is advised for the efficiency versus flow curve. However, different characteristic curve shapes, such as rising, steep, flat, or drooping require alternative functional relationships. A useful reference for adjusting viscous curves is the baseline with water, applying the same functional relationship as the reference curve. Once the functional relationship is selected, the regression of the curve can be performed using any available software or numerical methodology.

Moreover, the BHP required to drive the pump under viscous flow can be calculated for points 2′ to 5′ since the head, flow rate, and efficiency are known:

$$\mathrm{BHP}_{vis} = \frac{\rho g H_{vis} Q_{vis}}{\eta_{vis}} \tag{23}$$

The proposed model captures the experimental trends observed by Monte Verde et al. (2023) regarding the influence of fluid viscosity and rotational speed on ESP performance degradation. Increasing fluid viscosity significantly reduces the pump head and efficiency due to elevated internal energy dissipation. Conversely, increasing rotational speed mitigates performance degradation by raising the Reynolds number and thus reducing the friction factor. Overall, higher rotational speeds tend to improve ESP performance under viscous flow conditions, particularly within moderate viscosity ranges. The dimensionless parameter B, used in the proposed correlations, effectively incorporates the combined effects of viscosity and rotational speed, allowing the model to predict performance degradation trends observed in the experimental data. In addition, the specific speed of the pump also plays an important role in the sensitivity of ESP performance to fluid viscosity. Pumps with lower specific speeds are more susceptible to performance degradation under viscous conditions. The reduced passage size increases the impact of viscous shear forces, leading to greater head loss and efficiency reduction. In contrast, pumps with higher specific speeds, characterized by more axial designs, generally exhibit better tolerance to viscosity effects. Therefore, the degradation in head and efficiency due to increased fluid viscosity tends to be more pronounced in low-specific-speed pumps, an effect that is well captured by the proposed model.

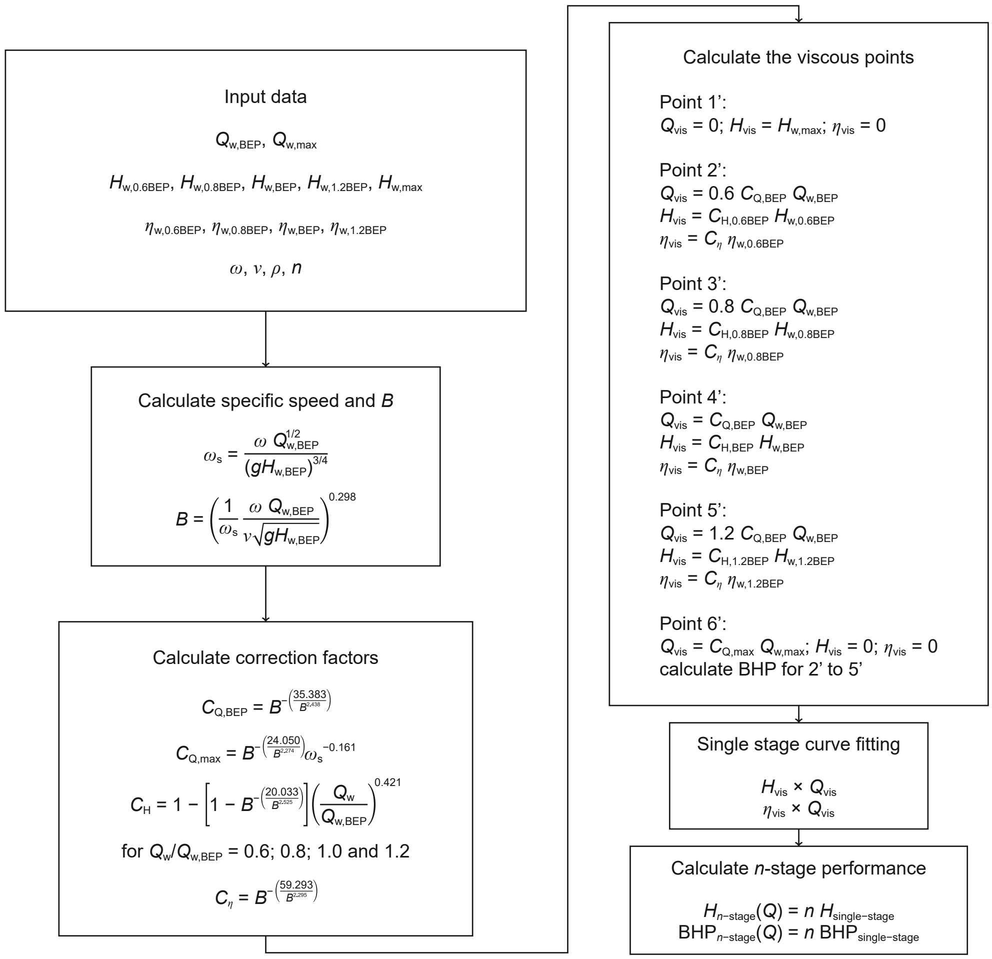

Fig. 2. Flowchart for predicting ESP performance in isothermal flow.

2.3. Performance prediction for isothermal flow

Given that the performance prediction model was developed for a single stage and considering that ESPs naturally have multiple stages, one must extend the application of the model to this scenario. A simple approach is to assume isothermal flow, which results in constant fluid properties throughout the ESP stages. Therefore, since the kinematic viscosity remains constant, all stages have the same performance. The viscous head and BHP of an n-stage ESP can be calculated by multiplying these characteristics by the number of stages. In turn, the efficiency does not change for an n-stage ESP. The flowchart in Fig. 2 shows this methodology.

The validity of the isothermal flow hypothesis depends on the viscosity and number of stages. Generally, this approximation is applicable to ESPs operating under low viscous flow and with only a few stages, where the heating effect is negligible. However, for ESPs with tens or hundreds of stages, this assumption becomes invalid. Nonetheless, this approximation serves as an important reference to establish the lower limit for ESP performance under viscous flow. Without heating, the inlet viscosity, which is at its highest, remains constant throughout the stages, leading to the greatest performance degradation.

2.4. Performance prediction for adiabatic and non-isothermal flow

In scenarios with high viscosity and many stages, which consequently result in high BHPs, the pumped oil may experience significant heating due to viscous dissipation. This phenomenon considerably reduces the fluid viscosity along the ESP. Therefore,

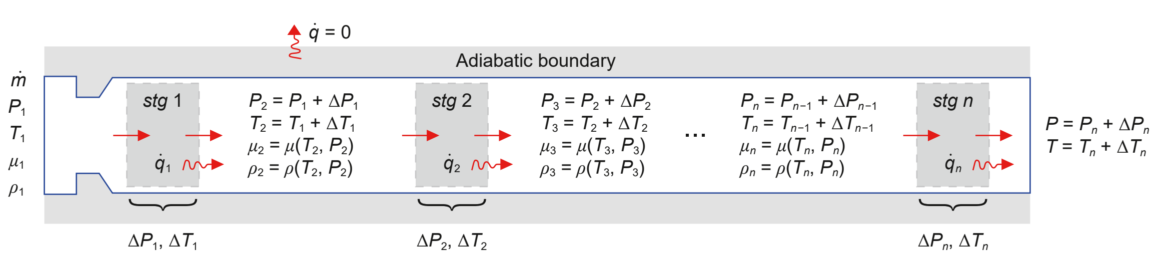

Fig. 3. Marching stage-by-stage procedure to calculate the ESP performance for adiabatic and non-isothermal flow.

assuming constant viscosity throughout the system can lead to errors in both sizing and performance prediction.

For a simplified approach, fluid heating can be estimated using the integral energy balance by considering a control volume that encloses an ESP stage (Monte Verde et al., 2021). Assuming non-isothermal, adiabatic, and incompressible flow of a single-phase fluid, and disregarding variations in kinetic and potential energy, the energy balance for this control volume results in:

$$\mathrm{BHP} = \dot{m}(h_2 - h_1) \tag{24}$$

where $\dot{m}$ is the mass flow rate and h is enthalpy. Rewriting Eq. (24) in terms of internal energy (u) variation between stage inlet (1), outlet (2), and flow work ($P\vartheta$), we have:

$$\mathrm{BHP} = \dot{m}(u_2 - u_1) + \dot{m}\vartheta(P_2 - P_1) \tag{25}$$

For an incompressible fluid, the variation of internal energy is a function of temperature, and recognizing that the term $\dot{m}\vartheta(P_2 - P_1)$ represents the useful power delivered to the fluid (P_h):

$$\dot{m}c_P\Delta T = \mathrm{BHP} - P_h \tag{26}$$

where c_P is the specific heat and ΔT is the temperature variation from stage inlet to outlet, given by the difference $T_2 - T_1$.

In Equation (26), fluid heating can be interpreted as a result of ESP inefficiency, where the difference between the energy used to drive the pump (BHP) and the useful power (P_h) delivered to the fluid is converted into thermal energy. Although this thermal energy does not contribute to lifting the fluid, it can be beneficial in some cases, as heating reduces the oil's viscosity, thereby decreasing performance degradation and increasing pump efficiency. By substituting Eq. (10) for 26, the fluid heating throughout the stage can be expressed as a function of the common operational parameters of the pump:

$$\Delta T = \left(\frac{1}{\eta} - 1\right)\frac{\Delta P}{\rho c_P} \tag{27}$$

For an n-stage ESP, a marching algorithm can be used to evaluate the BHP and total head. In this approach, the fluid properties are corrected stage by stage due to the temperature increase, as illustrated in Fig. 3. Eq. (27) is applied to each stage to calculate the temperature and estimate the viscosity at the stage outlet and, subsequently, at the inlet of the downstream stage. The fluid heating depends on the stage's efficiency and head, both of which are flow rate-dependent. Therefore, this procedure must be carried out for a constant flow rate. A given flow rate determines the stage's efficiency and head, and consequently the heating, which enables the calculation of viscosity at the inlet of the next stage.

Since the proposed prediction model provides degraded performance curves, a new curve must be determined for each corrected viscosity, based on a constant flow rate. In this way, the total head for a given flow rate is calculated by summing the heads of each stage. The efficiency corresponding to this flow rate is calculated from the sum of the BHP for each stage. The flowchart in Fig. 4 illustrates this procedure.

Starting from the operating conditions with water, rotational speed, and the fluid viscosity at the ESP intake, the degraded curve for the first stage is calculated using the procedure illustrated in Fig. 2. By defining a flow rate increment, δ, the head and efficiency for the given flow rate are calculated using the adjusted equations for $H_{\mathrm{vis}} \times q_{\mathrm{vis}}$ and $\eta_{\mathrm{vis}} \times q_{\mathrm{vis}}$, allowing for the estimation of the temperature at the stage outlet and, consequently, the calculation of the viscosity at the inlet of the next stage. After marching through all n stages, the total head and BHP are calculated as the sum of the head and BHP for each stage at the fixed flow rate. The average efficiency can be calculated based on the total head and BHP, assuming a constant average density throughout the ESP. The flow rate is then incremented and the process is restarted. This procedure is repeated for all flow rates to reconstruct the entire curve for the n-stage ESP. The fluid density varies little with temperature but is recalculated at the inlet of each stage, similar to the viscosity.

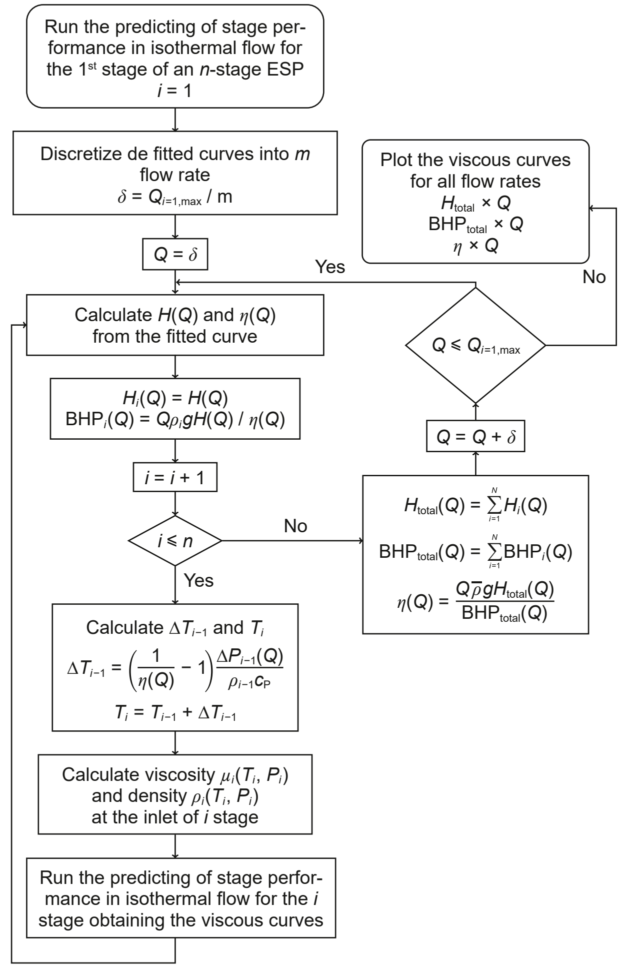

Fig. 4. Flowchart for predicting ESP performance in non-isothermal flow.

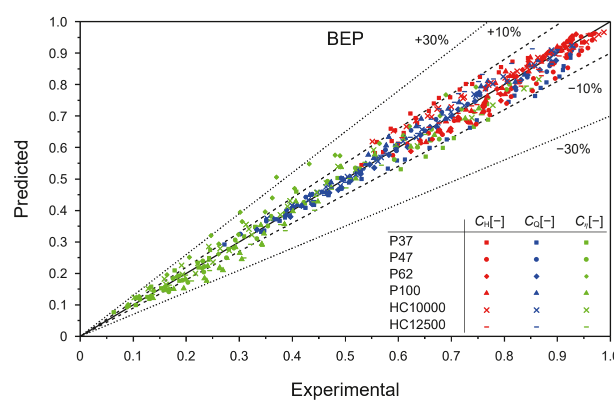

Fig. 5. Comparison between experimental and predicted head, flow rate, and efficiency correction factors at the BEP for different ESP models, viscosities and rotational speeds within training dataset.

The head at shut-off can be calculated by multiplying the single-stage head by the number of stages, since it was assumed that the fluid viscosity does not change at this point. Alternatively, the shut-off head can be obtained by defining an infinitesimal flow rate increment, δ.

Although the adiabatic flow hypothesis is far from reality, it is important because it provides the upper limit of ESP performance. In this scenario, all the energy dissipation is converted into heat, with no losses to the environment, resulting in the lowest possible viscosity at the ESP outlet. Thus, the presented approaches of isothermal and non-isothermal adiabatic flow define the limits of the highest and lowest possible performance for the ESP in viscous flow. The exact point within this performance region at which the ESP operates requires a detailed analysis of the heat exchange of the entire system, which is generally not trivial.

3. Results

The results presented in this section are divided into three parts. First, the proposed model is evaluated against the experimental dataset used for its adjustment. Next, the model is validated by using it to predict the viscous performance of an ESP model outside the dataset, considering the isothermal approach. Finally, the performance prediction results for another ESP model, also outside the dataset, are presented using the non-isothermal adiabatic methodology.

3.1. Assessment of the prediction model

Fig. 5 shows the comparison between the experimental head, flow rate, and efficiency correction factors at the BEP, provided by Monte Verde et al. (2023), and those predicted by the proposed model. Regarding the dataset, the experimental uncertainties (U) associated with the calculation and/or measurement of head, flow rate, and efficiency are $U_H = 4.0\%$, $U_Q = 0.15\%$, and $U_\eta = 5.1\%$, respectively. Furthermore, the propagated uncertainties in the calculation of the correction factors are $U_{C_H} = 5.6\%$, $U_{C_Q} = 0.2\%$, and $U_{C_\eta} = 7.2\%$, respectively.

The predominance of red and blue points near the ideal line indicates that the model provides accurate predictions for both head and flow rate. Approximately 96% of the predicted head values and 99% of the predicted flow rate values fall within a $\pm 10\%$ deviation range. The efficiency prediction, represented by green points, is also satisfactory, with 99% of the points falling within the $\pm 30\%$ range, and 69% showing deviations of less than $\pm 10\%$ compared to the measured value.

Fig. 6 shows the comparison for points 2′, 3′, and 5′. The predictions show a level of accuracy similar to that of the BEP prediction. In terms of head prediction, 100%, 98%, and 85% of the predicted points for $C_{H,0.6,\mathrm{BEP}}$, $C_{H,0.8,\mathrm{BEP}}$, and $C_{H,1.2,\mathrm{BEP}}$, respectively, fall within the $\pm 10\%$ deviation range. Regarding flow rate prediction, 99% of the predictions in all three points lie within the $\pm 10\%$ deviation range. For efficiency prediction, 98% of the predicted points are within the $\pm 30\%$ deviation range, with around 67% of the points showing deviations under 10% compared to the measured values. The assessment of the maximum flow rate prediction is shown in Fig. 7. For this condition, good accuracy is observed, with 98% of the predicted values falling within the $\pm 10\%$ deviation range.

Table 4 presents the statistical evaluation of the predictions performed by the proposed model. This table shows the statistical parameters for each correction factor, i.e., C_H, C_Q, and C_η, as well as the global parameter, which combines the statistics calculated by considering all three correction factors provided for each operational condition. The statistics for isolated correction factors

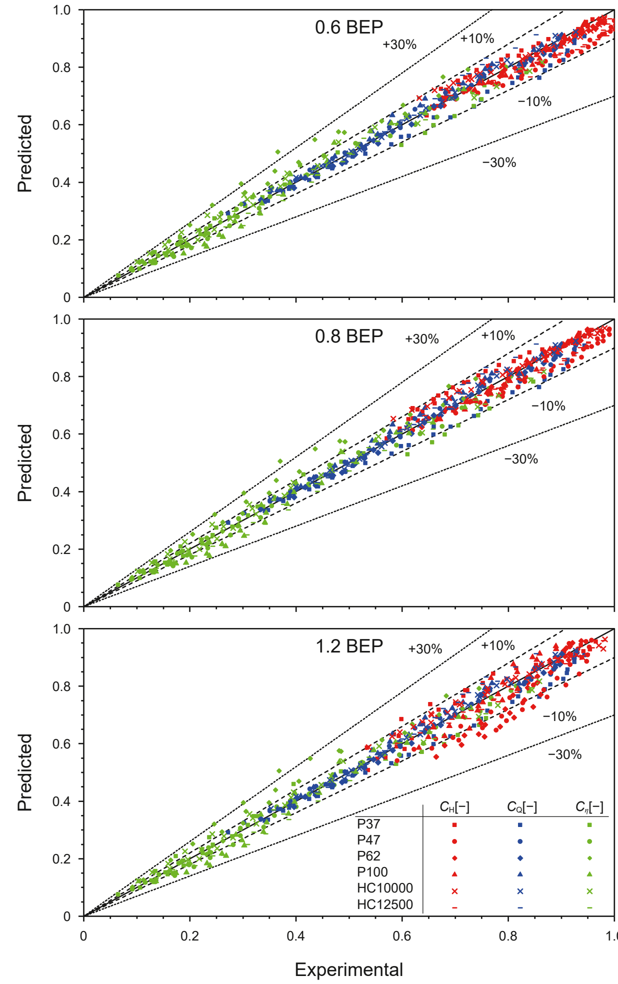

Fig. 6. Comparison between experimental and predicted head, flow rate, and efficiency correction factors at 60%, 80% and 120% of BEP for different ESP models, viscosity and rotational speeds within training dataset.

measure the model's ability to predict that specific variable. On the other hand, the global parameter indicates the model's accuracy in estimating the overall pump performance.

Considering the entire dataset, the application of the model demonstrates a global performance with MAPE ranging from 3.4%

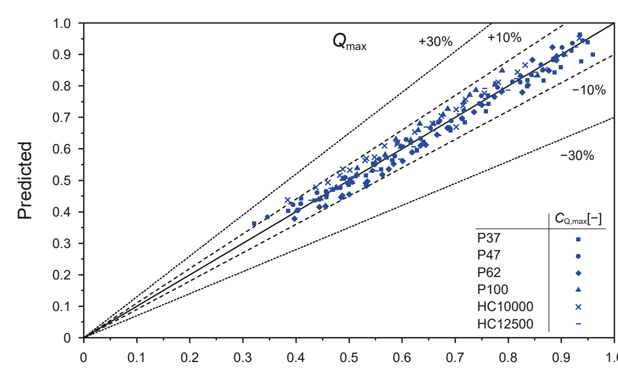

Fig. 7. Comparison between experimental and predicted flow rate correction factors at open flow for different ESP models, viscosity and rotational speeds within training dataset.

Table 4
Statistical evaluation of correction factors prediction by the proposed model.

		C_H	C_Q	C_η	Global
Point 2′ (0.6 BEP)	MAPE, %	3.4	3.2	8.3	5.0
	$e_{r,m}$, %	9.5	11.2	38.3	38.3
	RMSE [–]	0.036	0.028	0.036	0.034
	R^2 [–]	0.875	0.972	0.969	0.982
Point 3′ (0.8 BEP)	MAPE, %	3.4	3.2	8.2	4.9
	$e_{r,m}$, %	11.9	11.2	36.8	36.8
	RMSE [–]	0.034	0.028	0.037	0.033
	R^2 [–]	0.906	0.972	0.969	0.982
Point 4′ (BEP)	MAPE, %	3.9	3.2	8.3	5.1
	$e_{r,m}$, %	13.6	11.2	36.7	36.7
	RMSE [–]	0.035	0.028	0.037	0.034
	R^2 [–]	0.903	0.972	0.968	0.980
Point 5′ (1.2 BEP)	MAPE, %	5.2	3.2	8.4	5.6
	$e_{r,m}$, %	17.4	11.2	37.4	37.4
	RMSE [–]	0.051	0.028	0.037	0.040
	R^2 [–]	0.802	0.972	0.968	0.972
Point 6′ ($Q_{\max}$)	MAPE, %	–	3.4	–	3.4
	$e_{r,m}$, %	–	13.9	–	13.9
	RMSE [–]	–	0.026	–	0.026
	R^2 [–]	–	0.973	–	0.973

to 5.6%, a maximum error between 13.9% and 37.4%, RMSE between 0.026 and 0.040, and R^2 between 0.972 and 0.982. For the BEP, the model provides a reliable prediction, with global statistics showing a MAPE of 5.1%, a maximum error of 36.7%, an RMSE of 0.034, and an R^2 of 0.980. The predictions for head and flow rate are satisfactory. For the head correction factor, the MAPE ranges from 3.4% to 5.2%, with the maximum error ranging from 9.5% to 17.4%, an RMSE between 0.036 and 0.051, and an R^2 between 0.802 and 0.906. The flow rate correction factor predictions for the BEP, 0.6, 0.8, and 1.2 BEP points yield identical statistical parameters, with a MAPE of 3.2%, a maximum error of 11.2%, an RMSE of 0.028, and an R^2 of 0.972. This is because both the experimental data and the predicted points are equally proportional, according to the model's definition. The maximum flow rate estimation is also accurate, with a MAPE of 3.4%, a maximum error of 13.9%, an RMSE of 0.026, and an R^2 of 0.973. The efficiency prediction, while somewhat more complex, still delivers reliable results. Across all characteristic points, the efficiency correction factor predictions show a MAPE of approximately 8.3%, a maximum error of around 37.3%, and an RMSE and R^2 of approximately 0.037 and 0.969, respectively.

Fig. 8 shows the comparison between the viscous curves predicted by the model and the experimental curves for ESPs P37, HC12500, and P100, at viscosities of 50, 226, and 655 cP.

Cross markers indicate the experimental points, while triangle markers represent the characteristic points obtained by the model. The dashed curves result from the polynomial fitting performed using the six characteristic points predicted by the model. As suggested in Section 2.2, a quadratic polynomial fit was applied to the $H_{\text{vis}} \times Q_{\text{vis}}$ curves, and a cubic polynomial fit was applied to the $\eta_{\text{vis}} \times Q_{\text{vis}}$ curves.

To evaluate the accuracy of the predicted curves, the MAPE was considered. For each experimental flow rate, the measured head was compared with the head obtained at the same flow rate using the fitted curve equation. By applying this point-by-point procedure, the MAPE of each predicted head curve was obtained. The mean errors of the predicted efficiency curves, relative to the experimental efficiency curves, were calculated in a similar manner. The MAPE values for these curves are shown in Table 5.

The accuracy of the head curve prediction follows the same trend observed for the correction factors. The ability of the model to predict the head of ESPs operating with viscous fluid is

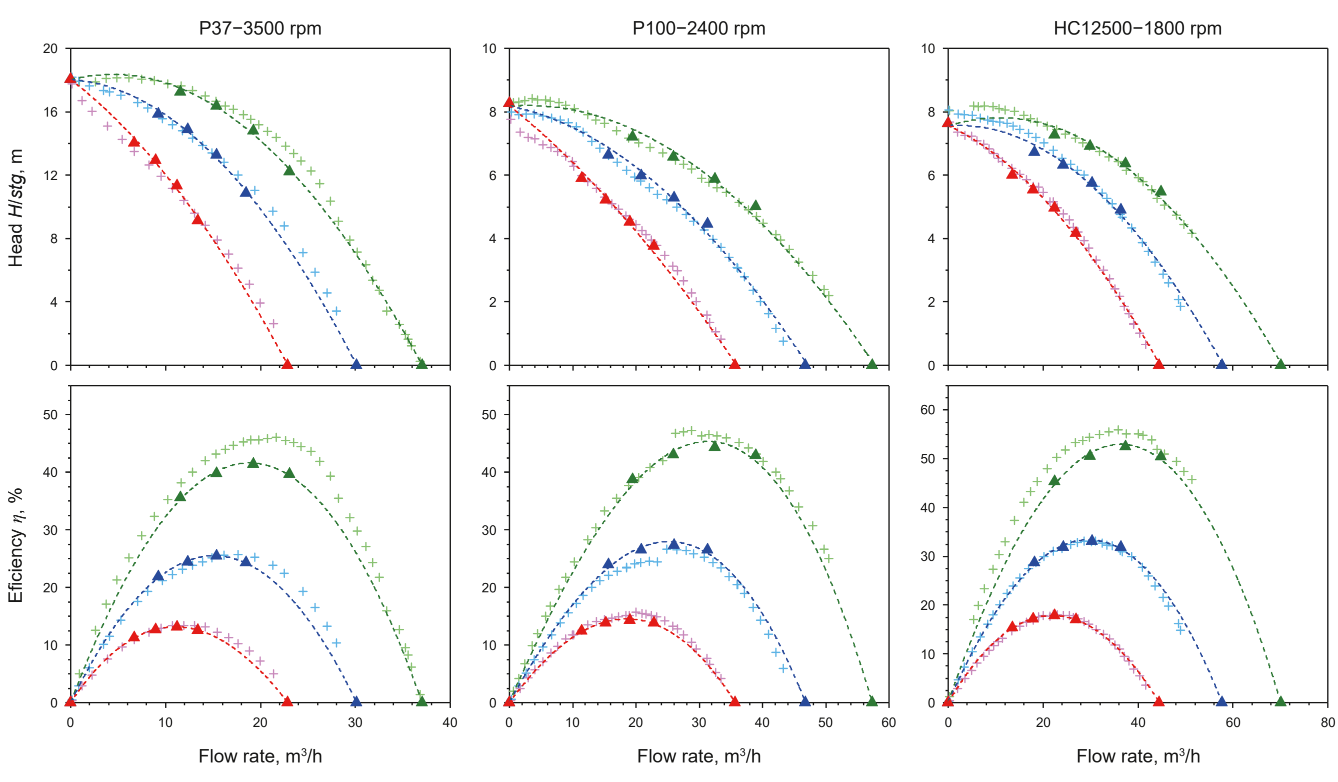

Fig. 8. Comparison between the viscous curves predicted by the model and the experimental curves for ESPs P37, HC12500, and P100, at viscosities of 50, 226, and 655 cP for different rotational speeds.

Table 5
Mean absolute percentage error (MAPE) for viscous curve prediction of ESPs P37, HC12500, and P100 at different rotational speeds and viscosities.

		50 cP	226 cP	655 cP
P37 – 3500 rpm	Head, %	4.1	6.1	7.9
	Efficiency, %	12.6	8.5	8.8
HC12500 – 1800 rpm	Head, %	1.9	3.9	3.6
	Efficiency, %	9.4	3.0	3.8
P100 – 2400 rpm	Head, %	2.7	4.6	5.9
	Efficiency, %	5.6	7.5	5.9

confirmed by the low MAPE values. These results are expected, as these data were used for model adjustment, as explained in Section 2.2. To validate the model's applicability outside the training dataset, predictions were made for the ESPs GN5200 and HC20000, as shown below.

3.2. Application of the prediction model for isothermal flow

This section presents the application of the proposed model to predict the viscous performance of the ESP GN5200, series 540, a three-stage pump with a specific speed of $\omega_s = 1.24$. The pump's performance under viscous flow was measured by Monte Verde (2016) and is not part of the dataset used to adjust the model. The experimental dataset includes inlet viscosities of 12, 33, 76, 114, 188, 251, 352, 471, 600, 836, and 1058 cP, along with rotational speeds of 2400, 3000, and 3500 rpm.

We highlight that, although the specific speed of $\omega_s = 1.24$ and the viscosity of 12 cP are outside the model's application range, the range of the independent parameter B varies from 5.17 to 21.35, which is close to the recommended range for the model's application, i.e., $4.76 < B < 19.02$.

For this test matrix, the authors report an average temperature increase of approximately 1 °C, which makes the assumption of constant viscosity reasonable. The proposed model was applied to predict the performance of the GN5200 across the entire test matrix using the isothermal flow approach.

Fig. 9 presents the comparison between the experimental and predicted correction factors for head, flow rate, and efficiency at the BEP, considering different viscosities and rotational speeds. The proximity of the points to the ideal 45° line highlights the model's accuracy in predicting the performance of the GN5200 at the BEP under various operating conditions. Considering all conditions of the experimental matrix, 100% of the predicted points fall within the ±30% deviation range. Among these, approximately 97% of the predicted points for head, 100% for flow rate, and 81% for efficiency exhibit deviations under ±15%.

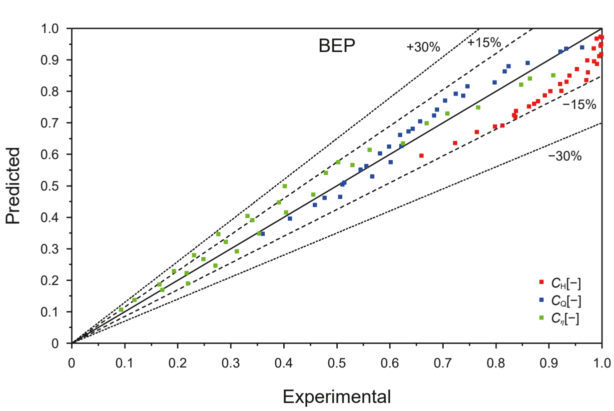

Fig. 9. Comparison between experimental and predicted head, flow rate, and efficiency correction factors at the BEP for ESP GN5200.

Table 6
Statistical evaluation of correction factors prediction by proposed model for ESP GN5200.

		C_H	C_Q	C_η	Global
BEP	MAPE, %	10.0	4.6	9.9	8.2
	$e_{r,m}$, %	15.0	9.3	25.1	25.1
	RMSE [–]	0.094	0.036	0.041	0.063
	R^2 [–]	−0.101	0.942	0.967	0.942

Table 6 presents the statistical parameters that evaluate the predictions of the correction factors for head, flow rate, and efficiency of the GN5200 at the BEP. The model provides a satisfactory prediction, with global performance at the BEP showing a MAPE of 8.2%, a maximum error of 25.1%, an RMSE of 0.063, and an R^2 of 0.942. For head prediction, despite the low R^2 and moderate RMSE, the mean error and maximum error remain low, with a MAPE of 10% and a maximum error of 15%. The predictions for flow rate and efficiency at the BEP are accurate, presenting MAPE values of 4.6% and 9.9%, maximum errors of 9.3% and 25.1%, RMSE values of 0.036 and 0.041, and R^2 values of 0.942 and 0.967, respectively.

Fig. 10 presents the comparison between the performance curves obtained experimentally and those predicted by the

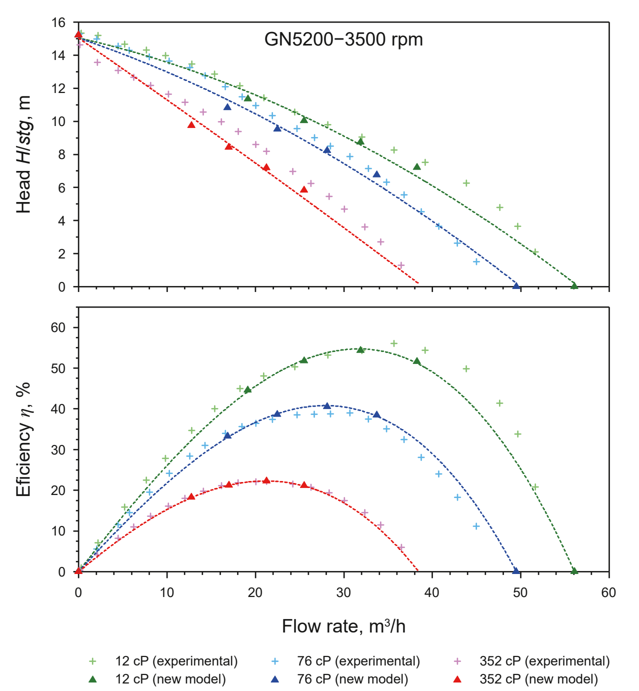

Fig. 10. Comparison between the performance predicted by the model using the isothermal approach, the fitted viscous curves based on these predicted points, and the experimental curves for ESP GN5200 at 3500 rpm with viscosities of 12, 76, and 352 cP.

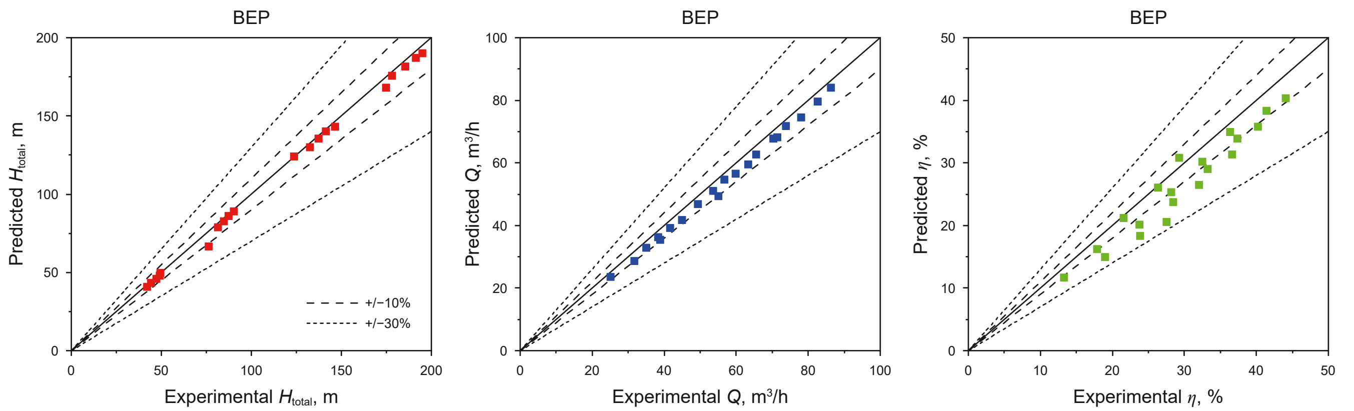

Fig. 11. Comparison between experimental and predicted head, flow rate, and efficiency at the BEP for ESP HC20000 considering the adiabatic and non-isothermal flow approach.

proposed model for the GN5200 ESPs at viscosities of 12, 76, and 352 cP, at 3500 rpm. In these results, polynomial adjustments of the 2nd and 3rd order were used for head and efficiency, respectively, to fit the discrete points (1′ to 6′) predicted by the model. Despite the pump's specific speed ($\omega_s = 1.24$) and the viscosity of 12 cP being outside the model's application range, the fact that the independent parameter B is, for the most part, within the recommended range results in good agreement between the predicted and experimental curves.

The mean error of the predicted curves is relatively low, ranging from 6.5% to 12.9% for head prediction and from 5.6% to 8.9% for efficiency prediction. The MAPE for each curve was calculated like the procedure used for the curves in Fig. 8.

3.3. Application of the prediction model for adiabatic and non-isothermal flow

This section presents the application of the proposed model to predict the viscous performance of the ESP HC20000, Series 675, a ten-stage pump with a specific speed of $\omega_s = 1.16$. The experimental characterization of the HC20000 viscous performance was conducted by Porcel et al. (2022). The experimental dataset includes inlet viscosities ranging from 230 to 1000 cP, along with rotational speeds of 1800, 2400, 3000, and 3500 rpm. Considering all operating conditions in the matrix, the value of the independent parameter B ranged from 5.66 to 21.82, which is close to the recommended range for the model's application.

Regarding the fluid heating as it flows through the pump, the authors report temperature increases of about 2 °C, reaching up to 15 °C in some cases, which significantly reduces the viscosity at the pump outlet. For example, operating at 3500 rpm with an inlet viscosity of 1000 cP, the average viscosity measured at the pump outlet was 739 cP, representing a reduction of 261 cP.

Therefore, assuming constant viscosity along the performance curve is inadequate, and the temperature change must be considered. The analysis of the head and efficiency of this 10-stage ESP can be performed using the marching procedure, following the non-isothermal approach described in Section 2.4.

Fig. 11 shows the comparison between the head, flow rate, and efficiency at BEP predicted by the model using the marching process under non-isothermal flow conditions and the results measured by Porcel et al. (2022). The results show the total pump head, considering all ten-stages. The model demonstrates good accuracy in its predictions, even for an ESP geometry outside the training dataset and with the simplifications of the adiabatic approach. For the prediction of total head at the BEP, 90% of the predicted points have errors within ±10%. For flow rate prediction at the BEP, 95% of the points fall within the ±10% deviation range. For efficiency prediction at the BEP, 100% of the points are within the ±30% deviation range, with 45% of deviations under ±10%. We also note that the model tends to provide an underestimated prediction, particularly for flow rate and efficiency.

Since the working fluid used in this simulation was crude dead oil, according to the experimental data of Porcel et al. (2022), it is important to note that its specific heat may vary depending on oil composition. Variations in specific heat can lead to noticeable changes in the predicted heating effect under non-isothermal flow conditions. Consequently, the applicability and accuracy of the proposed procedure rely on the use of a well-characterized and representative specific heat capacity for the analyzed fluid. Therefore, the results involving temperature rise and thermally coupled performance should be interpreted with appropriate caution, considering the model's sensitivity to this parameter.

The high accuracy of the predictions is confirmed by the statistical metrics presented in Table 7. The predictions for total head, flow rate, and efficiency of the HC20000 at the BEP, under different viscosities and rotational speeds, were analyzed. Notably, the mean errors for total head and flow rate are low, at 3.0% and 5.9%, respectively. Globally, when analyzing the prediction of the operational condition, the MAPE is 6.9%. Efficiency exhibits relatively higher uncertainties compared to head and flow rate, though they remain reasonable when compared to prediction models available in the literature. The MAPE for efficiency is 11.9%, with a maximum error of 25.6%.

To analyze the predicted head and flow rate curves, Fig. 12 shows a comparison with the experimental data at rotational speeds of 2400, 3000, and 3500 rpm, with viscosities ranging from 232 to 660 cP. In this figure, the cross markers represent the experimental data measured by Porcel et al. (2022) , while the triangle markers indicate the predictions using the procedure described in the flowchart of Fig. 4.

Table 7
Statistical evaluation of performance characteristics prediction by the proposed model for ESP HC20000.

		H_{total}	Q	η	Global
BEP	MAPE, %	3.0	5.9	11.9	6.9
	$e_{r,m}$, %	13.3	10.8	25.6	25.6
	RMSE [–]	3.830	3.194	3.851	3.638
	R^2 [–]	0.998	0.966	0.774	0.994

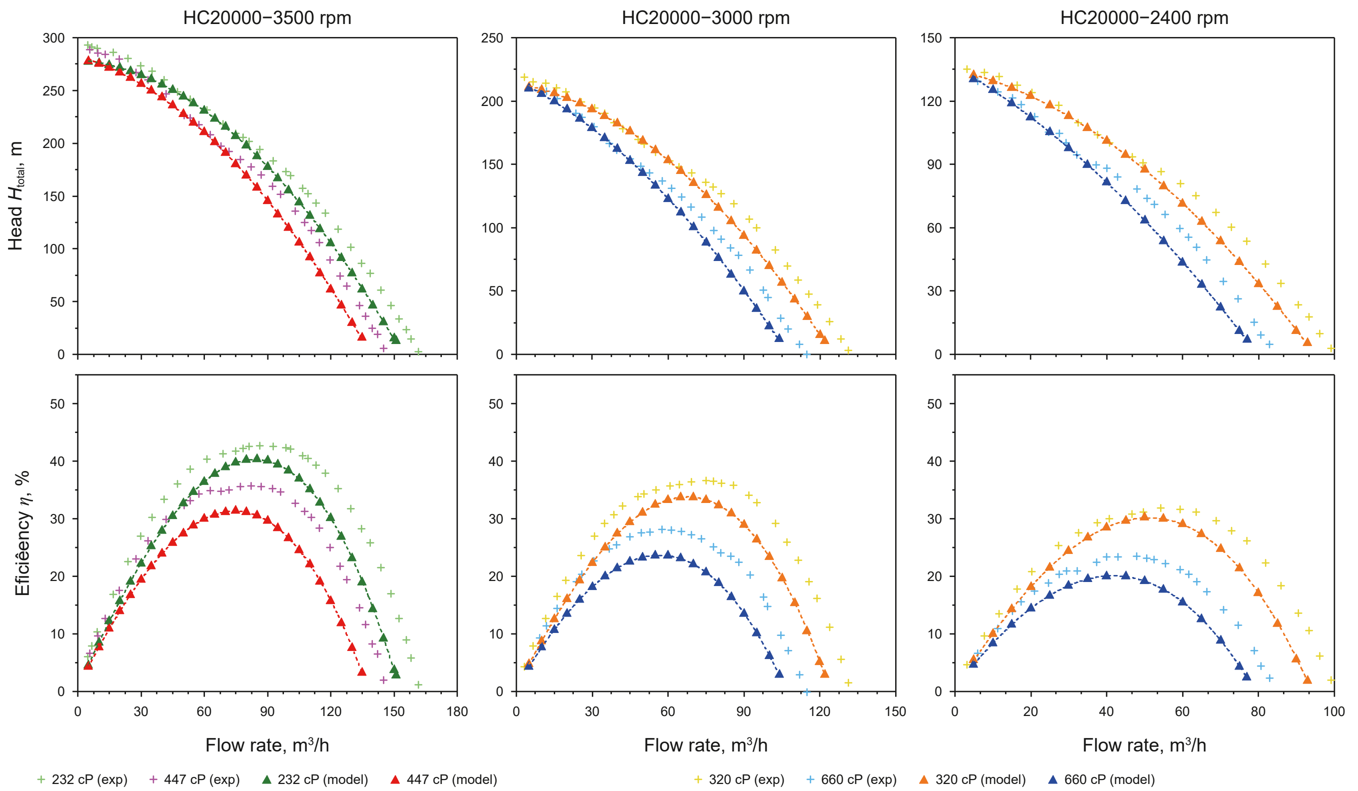

Fig. 12. Comparison between the performance predicted by the model using the adiabatic and non-isothermal approach, and the experimental curves for ESP HC20000 at 3500, 3000 and 2400 rpm in different viscosities.

Table 8
Mean absolute percentage error (MAPE) for viscous curve prediction of ESP HC20000 at 2400, 3000, and 3500 rpm and different viscosities.

		232 cP	447 cP
3500 rpm	Head, %	9.5	10.6
	Efficiency, %	16.8	14.0
		320 cP	**660 cP**
3000 rpm	Head, %	10.2	12.1
	Efficiency, %	18.9	23.6
2400 rpm	Head, %	11.6	16.3
	Efficiency, %	14.6	21.0

In general, prediction errors are smaller in the region between the shut-off and the BEP. Additionally, errors tend to increase with higher viscosities. The predicted curves also confirm that the model tends to underestimate viscous performance. Table 8 shows the MAPE for predicted curves, which were calculated similarly to the procedure used for the curves in Fig. 8. Analyzing the MAPE of the curve allows for an assessment of the prediction across the entire flow rate range, rather than focusing solely on the BEP.

Beyond its predictive performance, it is important to highlight the practical aspects of implementing the proposed model in real-world applications. The proposed model was specifically developed to balance predictive accuracy with practical applicability. Its analytical structure, based on correction factors applied to standard water performance curves, allows for straightforward implementation using simple algebraic calculations. This characteristic enables easy integration into existing pump selection and design software without the need for complex numerical solvers or high computational cost. In addition, the model can be incorporated into user-defined functions within reservoir simulators or production optimization tools, thus facilitating its use in field applications for ESP sizing, performance monitoring, and operational planning. These aspects reinforce the practical relevance of the model for ESP operations.

For clarity and reproducibility, Appendix A presents a worked example illustrating the calculation procedure used in the proposed methodology. The example details the stage-by-stage calculation of pump performance under non-isothermal flow conditions, including the evaluation of head, efficiency, temperature rise, and power for each stage.

4. Conclusions

This study proposes and evaluates a novel performance prediction model designed specifically for ESPs. The model estimates characteristic curves for head, brake horsepower (BHP), and efficiency. The following conclusions were obtained.

- The developed model proved to be an effective tool for predicting the ESPs performance under viscous flow conditions, demonstrating greater accuracy compared to models available in the literature, even when applied to pump geometries outside the calibration dataset. In addition to improved accuracy, another advantage provided by the model is its ability to predict multiple points on the performance curve, enabling its reconstruction. In general, most models available in the literature focus solely on predicting the BEP, which is insufficient for a comprehensive performance characterization.
- The accuracy achieved by the predictions is noteworthy due to the simplicity of the proposed model. The model is analytical and does not require complex detailing of the ESP geometry,

relying only on water performance data and specific speed as input parameters. This facilitates the implementation of the model in flow simulation software commonly used for production system design. Furthermore, such modeling is valuable for applications where the ESP is employed as a virtual flow meter, such as in production allocation scenarios.
- The prediction model was developed for a single stage, offering flexibility for its application in scenarios involving multiple stages. Extending the model to multiple stages is closely associated with the heating of the fluid as it flows through the ESP. This study presented two methodologies: one assumes no heating occurs, while the other considers all irreversibilities to be converted into fluid heating. These approaches provide a probable performance range for the ESP. However, given the diverse scenarios in which ESPs are applied, a thermal analysis is recommended to assess the fluid heating during pumping. Once the fluid heating is quantified, the proposed model can be applied iteratively, as demonstrated in this study.

Despite significant advances, it is important to highlight the limitations of the present model. This includes detailed analyses of heat exchanges and their effects under more extreme conditions to enhance predictive capability. In this sense, a key parameter to be addressed is the fluid heating during pumping, as temperature directly affects viscosity. This is a particularly complex task due to the wide variety of installation configurations in which ESP systems are employed, each with distinct thermal behaviors. Moreover, the current model is restricted to single-phase liquid flow and does not account for the presence of free gas in the pump; therefore, its application is recommended only for suction pressures above the oil's bubble point pressure. Extending the model to incorporate multiphase flow conditions remains a relevant direction for future research. recent developments in ESP technology suggest potential applications at high rotational speeds. The proposed model was developed for operating speeds up to 3500 rpm and captures the observed trend of increasing efficiency with speed. However, it is currently not possible to evaluate whether this trend continues beyond 3500 rpm. Experimental studies at higher speeds are needed to validate and extend the model for such conditions. Finally, future research should also consider coupling the model with thermal and multiphase flow simulations, aiming for more comprehensive and robust performance predictions under a broader range of operating scenarios.

CRediT authorship contribution statement

William Monte Verde: Writing – review & editing, Writing – original draft, Validation, Project administration, Methodology, Investigation, Formal analysis, Conceptualization. **Ellen Kindermann:** Writing – original draft, Validation, Methodology, Investigation, Formal analysis, Conceptualization. **Natan Augusto Vieira Bulgarelli:** Writing – review & editing, Conceptualization. **Bernardo Foresti:** Writing – review & editing, Supervision. **Antonio Carlos Bannwart:** Writing – review & editing, Supervision.

Data and code availability

The experimental dataset used in this study is available at Monte Verde et al. (2022). The computational scripts developed for this study are available from the corresponding author upon request.

Acknowledgments

The authors would like to thank PETROBRAS (Petróleo Brasileiro S/A), Brazil grant No: 2017/00764-1 and ANP ("Commitment to Research and Development Investments") for providing financial support for this study. The authors also thank the Artificial Lift & Flow Assurance Research Group (ALFA) and the Center for Energy and Petroleum Studies (CEPETRO), all part of the University of Campinas (UNICAMP).

Appendix A. Example calculation for the prediction model under adiabatic and non-isothermal flow

To illustrate the calculation process used in the proposed methodology, this appendix presents a concise worked example of the iterative procedure used to predict pump performance under non-isothermal flow conditions. For this example, the ESP HC20000, series 675, with ten stages was used. When operating with water at a rotational speed of 3447 rpm, the performance characteristics of this pump are presented in Table 9.

Step 1: As shown in the flowchart of Fig. 4, the initial step consists of predicting the performance for a single-stage under isothermal flow conditions. So, this first step corresponds to applying the complete calculation procedure described in the flowchart of Fig. 2, which includes the evaluation of head, and efficiency using the adiabatic assumption. For this purpose, in addition to the data presented in Table 9, the required input parameters are the rotational speed, viscosity, and density: 3447 rpm, 445 cP, and 936 kg/m^3, respectively. These values result in a kinematic viscosity of 4.75×10^{-4} m^2/s at an inlet temperature of 40.2 °C. The dimensionless specific speed and the B parameter are:

$$\omega_S = \frac{360.97 \times \sqrt{0.03154}}{(9.81 \times 21.37)^{3/4}} = 1.164$$

$$B = \left(\frac{1}{1.164} \times \frac{360.97 \times 0.03154}{4.75 \times 10^{-4}\ \sqrt{9.81 \times 21.37}}\right)^{0.298} = 8.700$$

Calculating the correction factors:

$$C_Q = 8.700^{-\left(\frac{35.383}{8.700^{2.438}}\right)} = 0.676$$

$$C_{Q,\max} = 8.700^{-\left(\frac{24.050}{8.700^{2.274}}\right)} \times 1.164^{-0.161} = 0.667$$

$$C_{H,0.6\mathrm{BEP}} = 1 - \left[1 - 8.700^{-\left(\frac{20.033}{8.700^{2.525}}\right)}\right] \times 0.60^{0.421} = 0.865$$

$$C_{H,0.8\mathrm{BEP}} = 1 - \left[1 - 8.700^{-\left(\frac{20.033}{8.700^{2.525}}\right)}\right] \times 0.80^{0.421} = 0.847$$

$$C_{H,\mathrm{BEP}} = 1 - \left[1 - 8.700^{-\left(\frac{20.033}{8.700^{2.525}}\right)}\right] \times 1.00^{0.421} = 0.832$$

$$C_{H,1.2\mathrm{BEP}} = 1 - \left[1 - 8.700^{-\left(\frac{20.033}{8.700^{2.525}}\right)}\right] \cdot 1.20^{0.421} = 0.819$$

$$C_\eta = 8.700^{-\left(\frac{59.293}{8.700^{2.295}}\right)} = 0.409$$

Calculating the viscous points:
Point 1':

$$Q_{vis} = 0$$

$$H_{vis} = 28.26 \text{ m}^3/\text{h}$$

$$\eta_{vis} = 0$$

Point 2':

$$Q_{vis} = 0.6 \times 0.676 \times 113.56 = 46.04 \text{ m}^3/\text{h}$$

$$H_{vis} = 0.865 \times 25.21 = 21.79 \text{ m}$$

$$\eta_{vis} = 0.409 \times 63.0 = 25.74\%$$

Similarly, by performing the same calculations for Points 3′, 4′, 5′ and 6′, the results are summarized in Table 10.

Finally, by performing single-stage fitting for head and efficiency, using second and third-order polynomials, respectively, the following curves were obtained for the 1st stage:

$$H_1 = -0.00109Q^2 - 0.05449Q + 27.84106$$

$$\eta_1 = -1.86720 \times 10^{-5}Q^3 - 0.00270Q^2 + 0.71097Q + 0.05020$$

where head is in meters, efficiency in %, and flow rate in m^3/h.

The results obtained from this isothermal analysis for the 1st stage are then used as the initial condition for the non-isothermal iteration.

Step 2: By discretizing the fitted curves into intervals of, for example, 15 m^3/h, it is possible to calculate the heating throughout the stages. For $Q = 15 \text{ m}^3/\text{h}$, the head and efficiency for the 1st satge is:

$$H_1 = 26.78 \text{ m}$$

$$\eta_1 = 10.04\%$$

After calculating the BHP and assuming $c_p = 1750 \text{ J/(kg} \cdot {}^\circ \text{C)}$, the heating throughout the 1st stage and the inlet temperature of the 2nd stage can be obtained:

$$\text{BHP}_1 = \frac{936 \times 9.81 \times 26.78 \times (15/3600)}{0.1004} = 1.019 \times 10^4 \text{ W}$$

$$\Delta T_1 = \left(\frac{1}{0.1004} - 1\right)\frac{2.456 \times 10^5}{936 \times 1750} = 1.34 \text{ °C}$$

$$T_2 = T_1 + \Delta T_1 = 40.2 + 1.34 = 41.54 \text{ °C}$$

Given the temperature at the inlet of the 2nd stage, it is possible to calculate the corrected viscosity and density. Using the temperature-dependent properties reported by Porcel et al. (2022), the fluid properties for the second stage are 405 cP, and 935 kg/m^3, respectively.

Step 3: Return to Step 1 and calculate the performance of the 2nd stage using the corrected properties from Step 2. Repeat this marching procedure throughout all stages while keeping the flow rate constant at. To illustrate, Table 11 presents the results of temperature and viscosity at the stage inlet, as well as the temperature increment, head, and BHP throughout the stages, at a flow rate of $Q = 15 \text{ m}^3/\text{h}$.

To obtain the complete curve, increase the flow rate by an increment ΔQ and repeat the entire procedure. Continue until reaching the maximum flow rate.

Table 9
ESP HC20000: Characteristic points on the water performance curve at 3447 rpm.

	Point 1	Point 2	Point 3	Point 4	Point 5	Point 6
Q_w, m^3/h	0	68.13	90.85	113.56	136.27	203.44
H_w, m	28.26	25.21	23.80	21.37	17.81	0
η_w, %	0	63.0	70.4	72.9	69.9	0

Table 10
ESP HC20000: Characteristic points on the viscous performance curve at 3447 rpm for the 1st stage.

	Point 1′	Point 2′	Point 3′	Point 4′	Point 5′	Point 6′
Q_{vis}, m^3/h	0	46.04	61.38	76.73	92.07	135.77
H_{vis}, m	28.26	21.79	20.16	17.78	14.58	0
η_{vis}, %	0	25.74	28.75	29.79	28.57	0

Table 11
ESP HC20000: Stage-by-stage results of the marching procedure under non-isothermal flow conditions at 3447 rpm.

	Stg 1	Stg 2	Stg 3	Stg 4	Stg 5	Stg 6	Stg 7	Stg 8	Stg 9	Stg 10
T_{inlet}, °C	40.20	41.54	42.86	44.15	45.42	46.66	47.88	49.09	50.27	51.44
μ_{inlet}, cP	445	405	369	338	310	285	263	243	225	208
ΔT_{stage}, °C	1.34	1.32	1.29	1.27	1.24	1.22	1.20	1.19	1.17	1.16
H_{stage}, m	26.78	26.89	26.98	27.07	27.15	27.22	27.28	27.34	27.39	27.44
BHP_{stage}, $10^4 \cdot$W	1.019	0.999	0.981	0.964	0.949	0.934	0.921	0.909	0.897	0.886

Nomenclature

B	independent dimensionless parameter, dimensionless
BHP	Break horsepower, Watt
C_H	head correction factor, dimensionless
C_Q	flow rate correction factor, dimensionless
C_η	efficiency correction factor, dimensionless
c_p	specific heat, kJ/kg·°C
e_r	absolute relative error, dimensionless, %
g	gravity acceleration, m/s^2
h	specific enthalpy, J/kg
H	head, m
$\dot{m}$	mass flow rate, kg/s
MAPE	mean absolute percentage error, dimensionless, %
P	pressure, Pa
P_h	hydraulic power, Watt
Q	volumetric flow rate, m^3/h
r_2	impeller outer diameter, m
R^2	coefficient of determination, dimensionless
Re_ω	rotational Reynolds number, dimensionless
RMSE	root mean squared error, the same unit of the analyzed parameter
T	temperature, °C
u	specific internal energy, J/kg
U	relative uncertain, %
ϑ	specific volume, m^3/kg
Γ	shaft torque, N·m
ΔP	pressure increment, Pa

η	efficiency, dimensionless, %
ρ	density, kg/m^3
ω	rotational speed, rpm
ω_S	specific speed, dimensionless
μ	dynamic viscosity, Pa·s or cP
ν	kinematic viscosity, m^2/s

References

ANSI-HI, 2010. Rotodynamic Pumps Guideline for Effects of Liquid Viscosity on Performance - 9.6.7-2010. Hydraulic Institute.

Bulgarelli, N.A.V., Biazussi, J.L., Monte Verde, W., Perles, C.E., de Castro, M.S., Bannwart, A.C., 2022a. Experimental investigation of the electrical submersible Pump's energy consumption under unstable and stable oil/water emulsions: a catastrophic phase inversion analysis. J. Petrol. Sci. Eng. 216, 110814. https://doi.org/10.1016/j.petrol.2022.110814.

Bulgarelli, N.A.V., Biazussi, J.L., Monte Verde, W., Perles, C.E., de Castro, M.S., Bannwart, A.C., 2022b. A novel criterion based on slip ratio to assess the flow behavior of w/o emulsions within centrifugal pumps. Chem. Eng. Sci. 247, 117050. https://doi.org/10.1016/j.ces.2021.117050.

Colodette, G., Pereira, C.A.G., Siqueira, C.A.M., Ribeiro, G.A.S.M., Rodrigues, R., de Matos, J.S., Ribeiro, M.P., 2008. Flow assurance and artificial lift innovations for jubarte heavy oil in Brazil. SPE Proj. Facil. Constr. 3, 1–8. https://doi.org/10.2118/117174-PA.

Costa, B.M.P., Oliveira, P.d.S., Roberto, M.A.R., 2013. Mudline ESP: eletrical submersible pump installed in a subsea skid all days. OTC–24201–MS. https://doi.org/10.4043/24201-MS.

Gülich, J.F., 2008. Centrifugal Pumps. Springer, Berlin Heidelberg, Berlin, Heidelberg. https://doi.org/10.1007/978-3-642-12824-0_1.

Homstvedt, G., Pessoa, R., Portman, L., Wang, S., Gonzalez, J., Maldaner, M., Margulis, J., 2015. Step-Change Seabed Esp Boosting Day 3 Thu. https://doi.org/10.4043/26141-MS. October 29, 2015, D031S034R002.

KSB, 1989. Kreiselpumpen-Lexiko. KSB.

Kumar, A., 2023. Perspectives of flow assurance problems in oil and gas production: a mini-review. Energy & Fuels 37, 8142–8159. https://doi.org/10.1021/acs.energyfuels.3c00843.

Lin, Y., Li, L., Yang, S., Chen, X., Li, X., Zhu, Z., 2024. Performance prediction and optimization of hydrogenation feed pump based on particle swarm optimization – least squares support vector regression surrogate model. Eng. Appl. Comput. Fluid Mech. 18, 2315985. https://doi.org/10.1080/19942060.2024.2315985.

Luo, H., Zhou, P., Cui, J., Wang, Y., Zheng, H., Wang, Y., 2025. Energy performance prediction of centrifugal pumps based on adaptive support vector regression. Eng. Appl. Artif. Intell. 145, 110247. https://doi.org/10.1016/j.engappai.2025.110247.

Monte Verde, W., 2016. Performance Modeling of ESP Pumps Performance Operating with gas-viscous Liquid Mixtures. Ph.D. thesis. University of Campinas. https://doi.org/10.47749/T/UNICAMP.2016.976346.

Monte Verde, W., Biazussi, J., Porcel, C.E., et al., 2021. Experimental investigation of pressure drop in failed Electrical Submersible Pump (ESP) under liquid single-phase and gas-liquid two-phase flow. J. Petrol. Sci. Eng. 198, 108127. https://doi.org/10.1016/j.petrol.2020.108127.

Monte Verde, W., Biazussi, J.L., Sassim, N.A., Bannwart, A.C., 2017. Experimental study of gas-liquid two-phase flow patterns within centrifugal pumps impellers. Exp. Therm. Fluid Sci. 85, 37–51. https://doi.org/10.1016/j.expthermflusci.2017.02.019.

Monte Verde, W., Kindermann, E., Biazussi, J.L., Estevam, V., Foresti, B.P., Bannwart, A.C., 2023. Experimental investigation of the effects of fluid viscosity on electrical submersible pumps performance. SPE Prod. Oper. 38, 1–19. https://doi.org/10.2118/210603-PA.

Monte Verde, W., Kindermann, E., Biazussi, J.L., Foresti, B.P., Estevam, V., Bannwart, A.C., 2022. Performance Database of Electrical Submersible Pumps (Esps) Under Viscous Fluid Flow. https://doi.org/10.25824/redu/AQX7SK.

Monte Verde, W., Kindermann, E., Bulgarelli, N.A.V., Pastre, L.F., Foresti, B., Bannwart, A.C., 2024. A critical analysis and improvements of empirical models for predicting the performance of electrical submersible pumps under viscous flow. Geoenergy Sci. Eng. 238, 212871. https://doi.org/10.1016/j.geoen.2024.212871.

Ofuchi, E., Cubas, J., Stel, H., Dunaiski, R., Vieira, T., Morales, R., 2020. A new model to predict the head degradation of centrifugal pumps handling highly viscous flows. J. Petrol. Sci. Eng. 187, 106737. https://doi.org/10.1016/j.petrol.2019.106737.

Porcel, C., Biazussi, J.L., Monte Verde, W., Estevam, V., Bannwart, A.C., Tavares, A., Santos, M.P.d.L., Rocha, P.S.d.M.V., 2022. Experimental study on the performance of electrical submersible pump operating with ultraviscous oil. SPE J. 27, 2470–2490. https://doi.org/10.2118/209221-PA.

Stel, H., Sirino, T., Ponce, F., Chiva, S., Morales, R., 2015. Numerical investigation of the flow in a multistage electric submersible pump. J. Petrol. Sci. Eng. 136, 41–54. https://doi.org/10.1016/j.petrol.2015.10.038.

Stepanoff, A., 1949. How centrifugals perform when pumping viscous oils. Power 93, 85–87.

Wang, H., Yang, Y., Xi, B., Shi, W.D., Wang, C., Ji, L.L., Song, X.Y., He, Z.M., 2024. Interstage performance and energy characteristics analysis of electric submersible pump based on entropy production theory. Pet. Sci. 21, 1354–1368. https://doi.org/10.1016/j.petsci.2023.10.032.

Xiao, J., Lastra, R., Roth, B.A., Lee, W., 2020. Material overview for electrical submersible pumps: part Ii—Polymeric and other materials. SPE Prod. Oper. 35, 9–17. https://doi.org/10.2118/198911-PA.

Yang, Y., Wang, H., Wang, C., Zhou, L., Ji, L., Yang, Y., Shi, W., Agarwal, R.K., 2024. An entropy efficiency model and its application to energy performance analysis of a multi-stage electric submersible pump. Energy 288, 129741. https://doi.org/10.1016/j.energy.2023.129741.

Zhou, P., Wen, Z., Wang, Y., Wu, Y., Wu, D., Huang, R., Yao, Z., 2025. Improving the energy performance of vortex pump based on whale optimization algorithm. Eng. Appl. Comput. Fluid Mech. 19, 2441344. https://doi.org/10.1080/19942060.2024.2441344.